Available online at www.sciencedirect.com
SCIENCE DIRECT
Coordination Chemistry Reviews 250 (2006) 1829–1841
COORDINATION CHEMISTRY REVIEWS
www.elsevier.com/locate/ccr

Review

Hemilabile coordination complexes for sensing applications

Sarah E. Angell [a], Cerrie W. Rogers [b,1], Yan Zhang [a], Michael O. Wolf [b], Wayne E. Jones Jr. [a,*]

[a] *Chemistry Department and Institute for Materials Research, State University of New York at Binghamton, Binghamton, NY 13902, United States*
[b] *Department of Chemistry, University of British Columbia, Vancouver, BC, Canada V6T 1Z1*

Received 10 March 2006; accepted 15 March 2006
Available online 30 March 2006

Contents

Abstract

Complexes containing hemilabile ligands provide a potential site for the reversible binding of analytes to a transition metal center because of their dynamic chelating ability. Due to their ability to reversibly bind analytes, hemilabile coordination complexes have recently been explored for application as small molecule chemosensors. Hemilabile complex sensors based on a Ru(II) bipyridyl system containing phosphine ether ligands have been shown to exhibit an analyte-dependent absorbance and emission response. When small molecule ligands such as water, acetonitrile, triethylamine, dodecanethiol and dimethylsulfamide (**L**) are in the presence of (**1**), an equilibrium forms between (**1**) and (**1**·**L**), the coordination complex resulting from substitution of the labile ether position. The binding of the Lewis bases creates dramatic changes in the photoluminescence. These photophysical changes are manifested as energetic shifts in the absorption and emission spectra, as well as changes in the temperature dependence of the emission lifetime. The photophysical characterization of ruthenium hemilabile complexes for the detection of moisture and small molecules is reported and analyzed in light of molecular orbital energy changes. It is shown that ruthenium hemilabile complexes hold potential as reversible sensors that exhibit ligand-dependent absorbance and luminescent signals.

Keywords: Ruthenium; Hemilabile; Temperature-dependence; Emission; Photophysics; Phosphine–ether; Luminescence; Bipyridyl; MLCT; Solvent dependence

* Corresponding author. Tel.: +1 6077772421; fax: +1 6077774478.
E-mail address: wjones@binghamton.edu (W.E. Jones Jr.).
[1] Present address: Department of Chemistry and Biochemistry, Concordia University, Montreal, Que., Canada H4B 1R6.

0010-8545/$ – see front matter © 2006 Elsevier B.V. All rights reserved.
doi:10.1016/j.ccr.2006.03.023

1. Introduction

1.1. Small molecules as sensors

Chemosensors have recently attracted a great deal of attention in the chemistry literature as analytical testing devices [1,2]. When a chemosensor is used for analytical purposes it will ideally give a qualitative indication of the presence of an analyte and a quantitative indication of analyte concentration. Examples of chemosensor signal outputs include color, fluorescence, conductivity or redox changes that may be monitored for the presence of a specific analyte.

There are several important factors to consider in the design of a chemosensor. A chemosensor must be selective toward a specific analyte and must not exhibit the same response in the presence of competing analytes. A chemosensor must also be sensitive; the signal that it produces must be easily identified. An ideal chemosensor is portable and its detection signal does not rely on extensive laboratory equipment. It is also desirable that a chemosensor produce quantifiable results so that not only the presence, but the quantity of analyte can be determined. A model chemosensor also exhibits characteristics of reversibility; the original signal should be restored in the absence of an analyte. Molecular sensors that exhibit these characteristics offer significant advantages over traditional bench top analytical instruments.

A multifunctional chemosensor that produces a selective, sensitive, quantitative, portable and reversible signal is desired. Many chemosensors have been developed in response to this need and may be classified into three general categories based on potentiometric [3–14], chromophoric [15–17] or fluorescent [18–28] readout signatures. Each of these classes of chemosensors has unique advantages.

Our approach to the development of this model chemosensor has included extensive investigation into the reversible and analyte-selective luminescence signaling response of Ru(II) bipyridyl complexes containing hemilabile phosphine ether ligands. We have found that an equilibrium forms between the coordinated form of the hemilabile complexes and an analyte-substituted form. More recently we have investigated the low temperature photophysical dependence of these systems and found that the hemilabile ligand complexes exhibit an analyte-dependent absorbance and emission response.

1.2. Coordination complex functionalized conjugated polymers

Eventually our interest in hemilabile coordination complexes will merge with our previous investigations of the sensitive, portable and quantitative signal properties of fluorescent conjugated polymers as chemosensors.

The development and success of fluorescent conjugated polymers as chemosensors that exhibit a sensitivity-enhanced transduction signal over their small molecule counterparts has been well established in previous publications. We have reported the synthesis and characterization of a fluorescence turn-off polymer, tolylterpyridine-poly[*p*-(phenyleneethynylene)-alt-(thienyleneethynylene). This polymer has been shown to undergo emission quenching in the presence of Ni^{2+} and Co^{2+} ions [29,30]. The resulting Stern–Volmer plots deviate positively from linearity as a result of the combined effects of static quenching and energy transfer along the polymer backbone. This bimodal behavior can be fit to an energy transfer enhanced Stern–Volmer equation which takes into account either the Dexter or Forster energy transfer mechanisms depending upon the specific analyte involved [30]. We have also reported the synthesis and characterization of the fluorescence turn-on polymers, *N*,*N*-diethylamino-PPETE and *N*,*N*,*N*′-trimethylethylenediamino-PPETE [26].

Many others have demonstrated the success of fluorescent conjugated polymers as chemosensors. Whitten and co-workers observed that [poly(2-methoxy-5-propyloxy sulfonate phenylene vinylene] exhibited greater than one million-fold fluorescence quenching sensitivity enhancement to methyl viologen compared to the corresponding small molecule fluorophore [14]. Swager and co-workers developed a selective and sensitive chemosensor for K^+ using a polymer with a poly(*p*-phenylene ethynylene) backbone and a crown ether receptor [31]. Wasielewski and co-workers have demonstrated both ionochromic and fluorescent transduction signals with 2,2′-bipyridyl-phenylene-vinylene-based polymers [32–34]. Schanze and co-workers also reports the fluorescence quenching of poly(phenylene ethynylene) substituted with anionic 3-sulfonatopropyloxy groups in the presence of differently sized cyanine dyes [35].

Given the enhanced sensitivity of conjugated polymer based chemosensors and the reversible selectivity of hemilabile ligand complexes, our interest lies in merging the hemilabile coordination complexes with our previous investigations of the sensitive, portable and quantitative signal properties of fluorescent conjugated polymers as chemosensors. The ultimate goal of this project is the development of a conjugated polymer containing a ruthenium hemilabile complex that would take advantage of the sensitive, portable and quantitative signal properties of the conjugated polymers and the reversible and selective signal of the hemilabile coordination complexes. It is proposed that this new chemosensor may be tuned to selectively respond to a wide range of analytes.

There is only one example to date of this type of strategy, though it uses a potentiometric response rather than fluorescence. Rheingold and Mirkin have made significant progress in the development of a hemilabile complex polymer. They have reported a hemilabile ruthenium complex containing a terthienyl group that can be polymerized at an oxidation potential that is lower than that of the Ru(II) center (Fig. 1) [36]. The advantage of such a system is that it contains an electronically controllable coordination sphere. Thus a relationship could be found between the small molecule uptake and release at the hemilabile center and the polymeric oxidation state. These systems are termed redox-switchable hemilabile ligands (RHLs) [37]. In an RHL, the labile portion of the hemilabile ligand is in electronic communication with a redox active group. Thus, the interaction between the labile portion of the ligand and the metal center

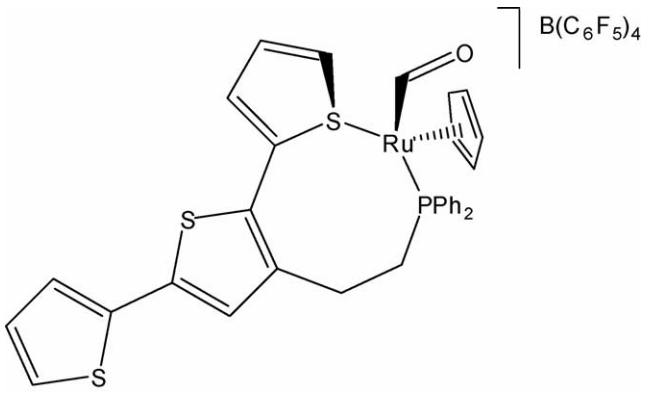

Fig. 1. A hemilabile complex integrated into a polymer backbone for the redox sensing of small molecules. Adapted from Ref. [36].

can be controlled through oxidation and reduction of the redox active group.

1.3. Hemilabile ligand complexes

Hemilabile ligands were first defined in 1978 by Jeffrey and Rauchfuss after investigating phosphine–amine and phosphine–ether ligands [38]. The hard ether and amine ligand components were found to dissociate from the softer metal center in the presence of small molecule substrates. Hemilabile ligands are polydentate chelates that contain both substitutionally inert and substitutionally labile groups. When incorporated into a transition metal complex, hemilabile ligands provide a potential site for the reversible binding of analytes to the metal center. Hard–soft acid–base interactions provide the basis for this hemilabile behavior. The labile group binds weakly to the transition metal center in the absence of small-molecule substrates. When a small molecule substrate binds to the metal center, the labile group remains in close proximity to the metal because of the inert ligand anchor. Re-coordination to the transition metal center occurs reversibly when the small molecule dissociates. Hemilabile coordination complexes have encountered success with applications in catalysis, small-molecule activation, small molecule sensing and stabilization of transition metal complexes [39].

The ability of the hemilabile ligand to re-coordinate in the absence of a bound small molecule makes hemilabile ligand coordination complexes ideal candidates for chemosensors. This reversibility distinguishes hemilabile complexes from other metal-based sensors. It is even possible to calculate equilibrium constants for the dynamic equilibrium that exists between the coordinated and the bound complexes [40].

The first use of a hemilabile ligand for a molecular sensor was demonstrated by Dunbar and co-workers. A phosphine ether ligand was attached to a Rh(I) core and found to reversibly bind carbon monoxide [41]. This hemilabile complex was placed within zirconia and titania glasses and subjected to spectroscopic and electrochemical probing. Cyclic voltammetry experiments exhibited a major change upon flushing the hemilabile composite film (cast on plantinum disk electrode) with CO. Significantly, after purging with nitrogen, the cyclic voltammogram returned to pre-CO conditions after 10 min.

While a number of review articles have been written that discuss the coordination of hemilabile ligands [39–43], we choose to highlight two. The first, written by Mirkin and co-workers, outlines five different classes of hemilabile ligands by the identity of the hemilabile functional group [39]. Hemilabile ligands are generally carbon based, nitrogen based, phosphorus based, arsenic based or chalcogen based (elements from Group VIB). The second review article, written by Baunstein and Naud [44], categorizes hemilabile ligands into three general groups based upon the mechanism by which the coordinated hemilabile complex forms the bound hemilabile complex. In compounds of *Type I Hemilability*, the hemilabile complex consists of a metal which has a variable coordination number and thus the equilibrium between the coordinated complex and the bound complex occurs within the same molecule; the ligand may be bound or it may be unbound, but in either case a guest molecule need not be present because the metal has a variable coordination number. Complexes of *Type II Hemilability* experience intramolecular competition. In this instance, the metal is not of variable coordination number and therefore equilibrium may result from two hemilabile moieties on the same metal center competing for one site. *Type III* complexes involve an external molecule that competes with the labile ligand–metal bond for coordination at the metal center. *Type III* complexes are most applicable for use as chemosensors.

Phosphine–ether ligands (PO) compose a particular class of hemilabile ligands that have drawn recent attention in the literature. Many papers that mention Ru(II) phosphine–ether (PO) complexes discuss primarily synthesis and characterization. For instance, Dutta and co-workers synthesized a group of PO Ru(II) complexes and solely investigated the prevalent isomeric molecular structure [45]. Some authors also mention possible applications. Werner and co-workers report the synthesis of a PO Ru(II) complex containing two bulky hemilabile ligands (Fig. 2) [46]. In the presence of the HBF_4, the ether portion of the hemilabile ligand is no longer coordinated to the metal center. A small molecule does not take its place; however a carbon based ligand that was formerly double bonded to the metal center assumes a triple bond to the metal center. This would be an example of a molecule exhibiting *Type II Hemilability*. Werner and co-workers proposes that these types of complexes may have applicability in olefin metathesis [46].

Lindner investigated a structurally diverse form of a phosphine–ether hemilabile ligand—a ligand that contained two

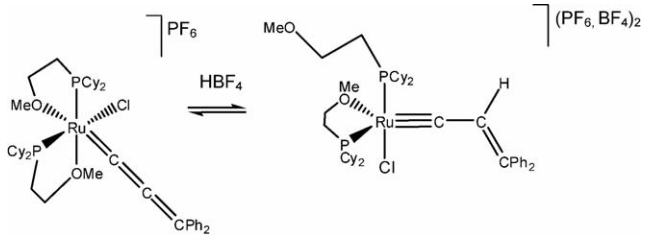

Fig. 2. An example of a PO hemilabile complex of *Type II Hemilability*. This complex has applications in olefin metathesis. Adapted from Ref. [46].

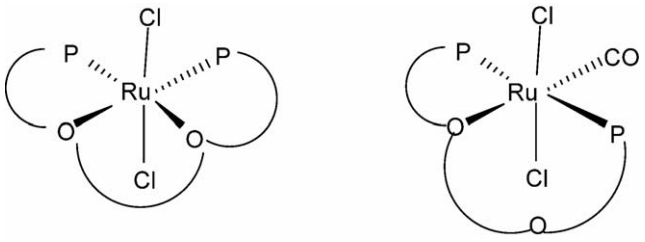

Fig. 3. A tetradentate phosphine–ether hemilabile complex. The compound on top is bound to CO; this binding was not found to be reversible as is the case with bidentate phosphine ether ligands. Adapted from Ref. [47].

centralized ether moieties and two external phosphine moieties, such that the ruthenium complex was coordinated to a tetradentate ligand, with two soft phosphorus chelates and two hard oxygen chelates and two monodentate chlorine atoms (Fig. 3) [47]. It was hoped that carbon monoxide may be activated at one of the labile ether sites of this tetradentate PO Ru(II) complex. Although this complex could exist as a tridentate complex with CO substituted in the ether labile position, the CO binding was not reversible. Attempts to activate the CO were not successfully demonstrated due to relative immobility of the ligand system and shielding of the reactive center.

1.4. Optically based hemilabile coordination complexes as molecular sensors

There is an absence of work, in the literature, dedicated to hemilabile sensors that include a luminescent signaling component. Chromophoric and luminescent signals are desirable as they are easily detected. In many instances, nothing beyond the human eye is needed to observe a color change that signals the binding of a certain molecule. Given both the dynamic binding abilities of hemilabile ligands and the ease of detection of chromophoric and luminescent signals, the development and analysis of such an optical-based hemilabile sensor is desirable.

Relatively few examples are found of hemilabile sensors that include a chromophoric signaling system, although the Rh(I) phosphine–ether complex developed by Dunbar and coworkers for carbon monoxide sensing exhibited a change in the absorbance spectra of the hemilabile complex in the presence and absence of CO [48].

We have demonstrated that the complexes $[Ru(bpy)_2L](PF_6)_2$ [L = (2-methoxyphenyl) diphenylphosphine (RuPOMe) (**1**) and (2-ethoxyphenyl)diphenylphosphine (RuPOEt) (**2**) (Fig. 4) exhibited analyte-dependent emission and colorimetric behavior [49]. Later, the complex $[Ru(bpy)_2L](PF_6)_2$ [L = (2-(2-propyoxy)phenyl)diphenylphosphine)] (RuPO^{i}Pr-P) (**3**) was also shown to exhibit small molecule sensing abilities [40]. These molecules reversibly bind various small molecules and can be monitored through changes in both the absorption and low temperature (77 K) emission spectra [49].

To our knowledge, this is the first example of a metal-to-ligand charge transfer (MLCT) based sensor designed to take advantage of the reversible binding provided by a hemilabile ligand. MLCT excited states are ideal as chemosensors because of their strong visible absorptions, long luminescence lifetime,

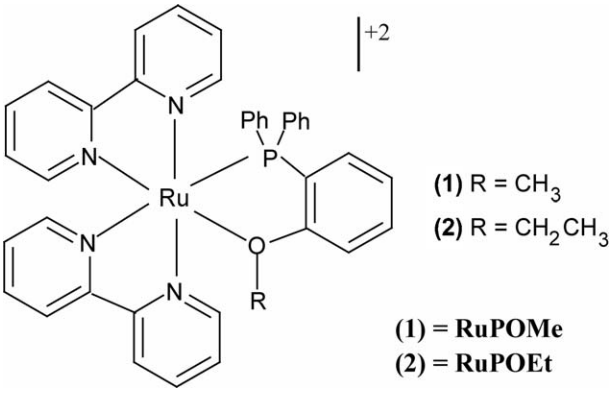

Fig. 4. $[Ru(bpy)_2L](PF_6)_2$ [L = (2-methoxyphenyl)diphenylphosphine (RuPOMe) (**1**) and (2-ethoxyphenyl)diphenylphosphine (RuPOEt) (**2**)].

and proclivity to both electron and energy transfer quenching processes [50–52].

2. Synthesis and structure

2.1. Synthesis of Ru(II) hemilabile coordination complexes

Complexes (**1**–**3**) were prepared by reacting $Ru(bpy)_2Cl_2{\cdot}2H_2O$ with two equivalents of $AgBF_4$ in acetone. The resulting complex $[Ru(bpy)_2(Me_2O)_2]^{2+}$, was reacted with one equivalent of the appropriate phosphine ether ligand [40,49]. Metathesis occurred with the addition of NH_4PF_6. The orange/yellow powders are soluble in polar organic solvents. The ^{1}H NMR spectra are characteristic. Signals corresponding to the aromatic ligands are spread over a broad range of the spectrum (δ 8.55–6.39) [49]. A lone upfield signal corresponds to the labile ether ligand.

2.2. X-ray crystallography studies

A single crystal of (**3**) has been reported. The ORTEP representation (Fig. 5) of the solid state molecular structure revealed that water was substituted at the labile position of the hemilabile coordination triclinic crystal [40]. The distances between the Ru(II) metal center and the various ligands averaged 2.13 Å. The geometry about the Ru(II) center was found to be a distorted octahedron. This was also found to be the case in the solid state when the POMe ligand of (**1**) and (**2**) were bound to the metal center [53]. In the discussions that follow, the molecular rotation about the Ru–P bond in the uncoordinated state is of importance in defining the ligand field states. The crystal structure may suggest that hydrogen bonding exists between the water coordinated to the metal center and the free ether.

3. Host–guest chemistry

3.1. $^{31}P\{^1H\}$ equilibrium studies: demonstration of reversibility

NMR spectra for (**1**) with the addition of H_2O were obtained at an approximate complex concentration of 10^{-3} M in 2:1

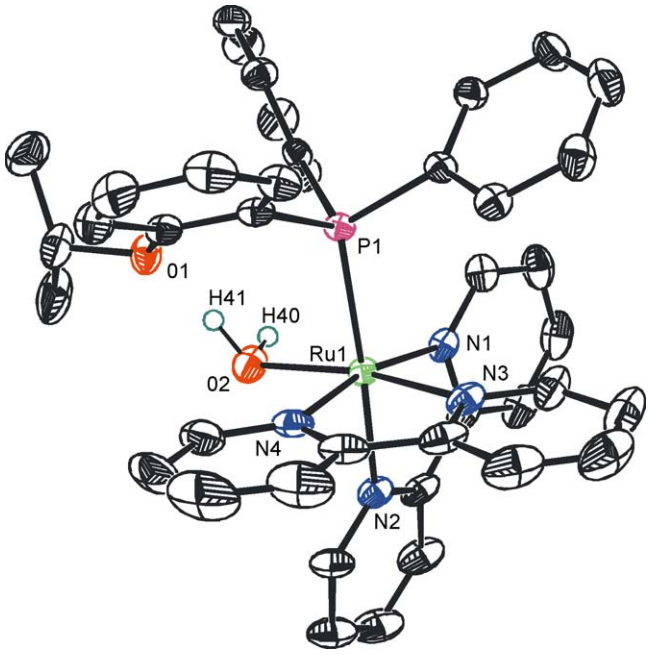

Fig. 5. ORTEP representation of hand-picked crystal, RuPO^{i}Pr-P. Hydrogen atoms and PF_6^- counterions are omitted for clarity.

ethanol/acetone. The ether-coordinated complex (**1**) shows a sharp singlet in the $^{31}P\{^1H\}$ NMR spectrum at δ 52.8. When water 5% (v/v) is added to (**1**), another singlet appears, δ 40.4, corresponding to the water bound-RuPOMe complex, denoted (**1**·H_2O).

The reversibility of the reaction of (**1**) with H_2O to form (**1**·H_2O) was established with $^{31}P\{^1H\}$ NMR spectroscopy. Complexes (**1**) and (**1**·H_2O) form an equilibrium in solution with rate constant, K, modified to $K_{eff} = K/\alpha = [\mathbf{1}\cdot H_2O]^2/([\mathbf{1}][H_2O])$ which includes the proportionality constant, α, that accounts for the fact that the ether is tethered to the metal and has a higher effective concentration than it would if it were free in solution. When $^{31}P\{^1H\}$ NMR is used to follow the titration of (**1**) with water, the integrated signals for (**1**) and (**1**·H_2O) may be used to calculate K_{eff}. When $[\mathbf{1}\cdot H_2O]^2/[\mathbf{1}]$ is plotted versus $[H_2O]$ a linear plot results with $K_{eff} = (6 \pm 3) \times 10^{-3}$. The reversibility of the hemilabile moiety was demonstrated when more (**1**) was added to solution and reestablishment of equilibrium was observed [40].

$^{31}P\{^1H\}$ NMR studies of (**3**) proved that the isopropyl ether ligand was more easily displaced by other solvent molecules than (**1**). Presumably this increased susceptibility to small molecules is due to steric constraints of the isopropyl ether group when it is coordinated to the metal center [40].

3.2. Photophysical characterization: demonstration of selective response

The photophysics and photochemistry of transition metal complexes with MLCT excited states have been studied extensively [54–59]. Emission from an excited Ru(II) polypyridyl complex, such as $[Ru(bpy)_3](PF_6)_2$ [(bpy) = 2,2′-bipyridine], commonly occurs from a triplet metal-to-ligand charge-transfer

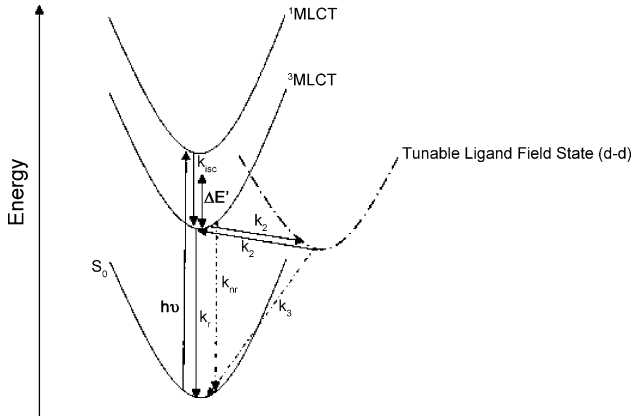

Fig. 6. Energy state diagram for (**1**) and (**2**) showing the possibility of a thermally populated d–d state that may be tuned by variations in the ligand field, where $\Delta E'$ is the activation energy barrier.

(^{3}MLCT) excited state [60–62]. Such a ^{3}MLCT state can also undergo internal conversion by thermal deactivation to a triplet, metal-centered ligand field (d–d) state with rate, $k' = k_2$ and activation energy barrier, $\Delta E'$ (Fig. 6). These low energy states do not usually appear in the absorbance or emission spectra because of very low extinction coefficients and low emission quantum yields. However, these states impact the photophysical and photochemical properties of the complexes because they provide an efficient pathway for non-radiative decay.

At ambient temperatures, the thermally populated d–d states of (**1**) and (**2**) provide a very efficient mechanism for non-radiative decay. This results in very short lifetimes and no room-temperature emission. Temperature-dependent lifetime measurements are used to obtain information regarding this metal-centered excited state. Temperature-dependent emission has been observed previously with complexes of the type $[Ru(bpy)_2L_2](PF_6)_2$ [60,62]. The energy of the ligand field state, and, likewise the rate and thermal activation energy barrier of the MLCT → d–d transition may be tuned through variations in the ligand, L [62–67]. Phosphine ligands, such as those in (**1**) and (**2**), are known to increase the thermal accessibility of d–d states, to the extent that luminescence from phosphine complexes is typically not measurable at room temperature [62]. At 77 K, luminescence is observed as thermal population of the non-radiative d–d state is effectively reduced due to the activation of the energy barrier. Emission is observed for the transition from the ligand π^* orbital back to the ruthenium ground state HOMO.

3.2.1. Absorbance and emission studies of (*1*) and (*2*)

RuPOMe (**1**) displays concentration dependent absorption and emission behavior [49,40]. In 2:1 ethanol/acetone solvent, the effect of going from 1.0×10^{-3} M solution to 3.0×10^{-5} M solution resulted in a 2.9×10^5 cm^{-1} red shift in the absorbance maxima and a 2.4×10^5 cm^{-1} red shift in the 77 K emission maxima. These spectral changes have been attributed to the fact that in the dilute solutions of (**1**), the relative ratio of H_2O to (**1**) is higher than in the concentrated solutions of (**1**). Indeed this red-

shifting phenomenon is observed when (**1**) is titrated with water [68]. The absorbance maxima for the spin-allowed MLCT electronic transition of (**1**) in 3.0×10^{-5} M 4:1 ethanol/methanol solution was observed at 454 nm. Consistent with the titration experiment mentioned above, variations in the atmospheric humidity have been observed to cause significant changes in the position of the MLCT band.

Similar fluctuations in the emission spectra of complex (**1**) have also been observed. The highest energy low-temperature emission band of (**1**) at 77 K is observed at $\lambda = 558$ nm corresponding to the bound-ether complex. On the lower energy side of this band there is a broad shoulder, $\lambda = 616$ nm, corresponding to the presence of the aquo complex (**1**·H_2O). These assignments have been supported by low temperature excitation spectra monitored at different wavelengths [68]. Analogous water-dependent red-shifts in both the absorbance and 77 K emission spectra have been observed for the RuPOEt (**2**) complex.

The MLCT emission bands of (**1**) and (**2**) are at higher energies than the MLCT emission band of $[Ru(bpy)_3](PF_6)_2$ (602 nm) [69–70]. This has been attributed to the presence of the π-accepting phosphine ligand, which enhances π-backbonding with the metal d-orbital in competition with the bipyridyl ligands. This molecular orbital interaction results in a stabilization of the metal-based HOMO as demonstrated by the higher energy MLCT transition.

Table 1
Gutmann solvent donor numbers

Ligand	Gutmann solvent donor number
CH_3CN[a]	14.1
Acetone	17
Ether	19.2
DMSO	29.8
Water[b]	33
TEA	61

Equal to $-\Delta H_{D\bullet SbCl_5}$ in kcal/mol. From Ref. [71].
[a] [81].
[b] [82].

Changing the chemical identity of the hemilabile phosphine ether from POMe to POEt does not cause a significant change in the MLCT transition energy. However, the addition of a small molecule ligand, such as H_2O, to the metal center, causes significant changes in the MLCT band. Recent studies involving the coordination of other small molecules to the metal center have confirmed the small-molecule ligand dependency of the energy gap.

3.2.2. *Absorbance properties of the host–guest complex (**1**·**L**)*

The absorbance properties of (**1**), at room temperature, were evaluated in the presence of several ligands (**L**). Table 1

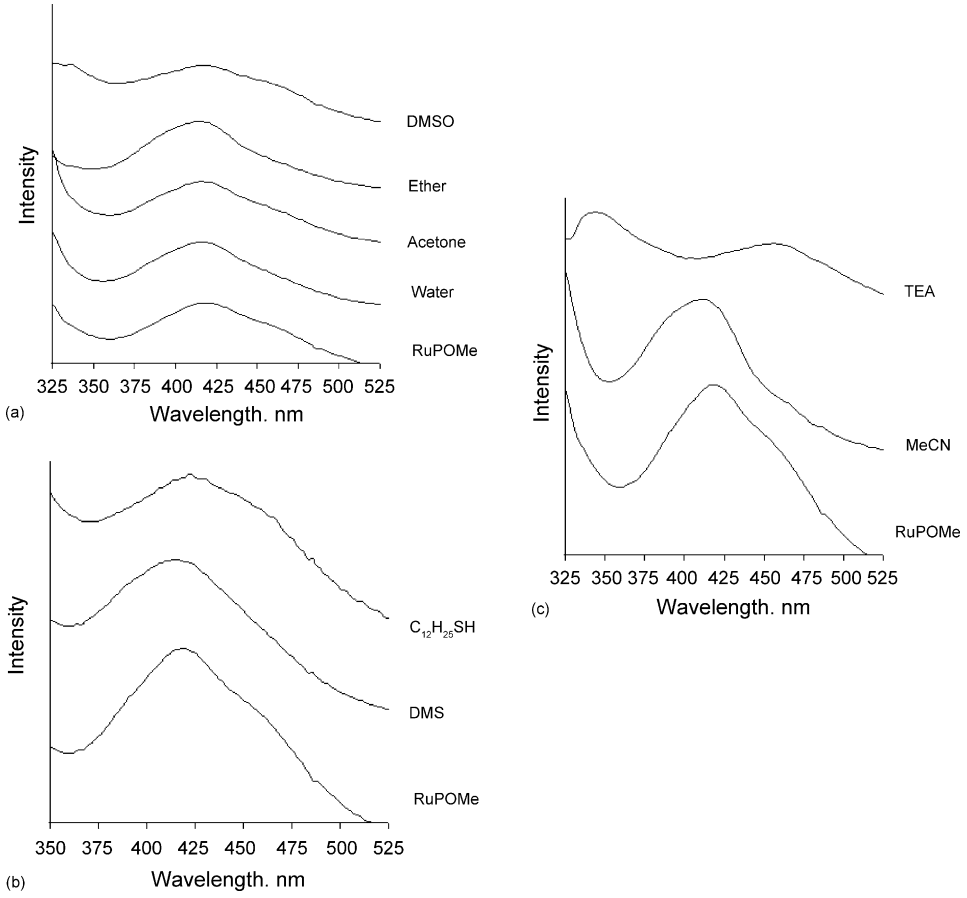

Fig. 7. Absorbance of (**1**) with 100 equivalents of various small molecules. (a) O-bound, (b) S-bound and (c) N-bound. Measurements were taken in a 4:1 EtOH:MeOH solution.

indicates the ligands that were used in this study, along with their absorption and emission energies.

The absorption spectra at 298 K for 3.0×10^{-5} M RuPOMe with 100 mol equivalents of a variety of O-bound analytes are displayed in Fig. 7a. The variations in the MLCT absorbance band for the other O-bound ligands are slight. There are only small shifts in the absorbance maximum of (**1**) when 100 equivalents of acetone and ether and DMSO are present.

The absorption spectra at 298 K for 3.0×10^{-5} M RuPOMe with 100 mol equivalents of two S-bound analytes are shown in Fig. 7b. The MLCT band for (**1**·DMS) appears to have a similar MLCT band to (**1**). The (**1**·$C_{12}H_{25}SH$) MLCT band is slightly red-shifted relative to (**1**). Fig. 7c displays the absorption spectra at 298 K for 3.0×10^{-5} M RuPOMe with 100 mol equivalents of the two N-bound analytes. The MLCT energy gap for (**1**·MeCN) is slightly blue shifted relative to (**1**). Interestingly, a 2.0×10^{5} cm^{-1} red shift is observed for the MLCT band of (**1**·TEA).

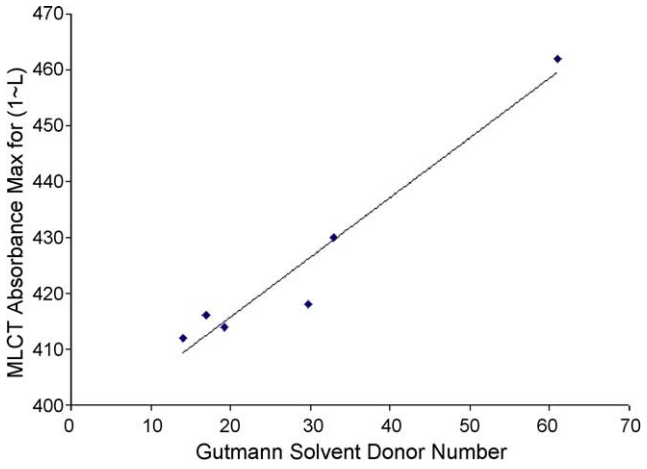

Fig. 8. MLCT dependence on the Gutmann solvent donor parameters with 100 M equivalents of **L** added to a 3.0×10^{-5} M solution of (**1**). The value reported for (**1**·H_2O) is for approximately 1000 M equivalents of **L** added to a 3.0×10^{-5} M solution of (**1**). Solvent donor numbers were not found for DMS or $C_{12}H_{25}SH$. **L**, from left to right = CH_3CN, acetone, ether, DMSO, water, TEA.

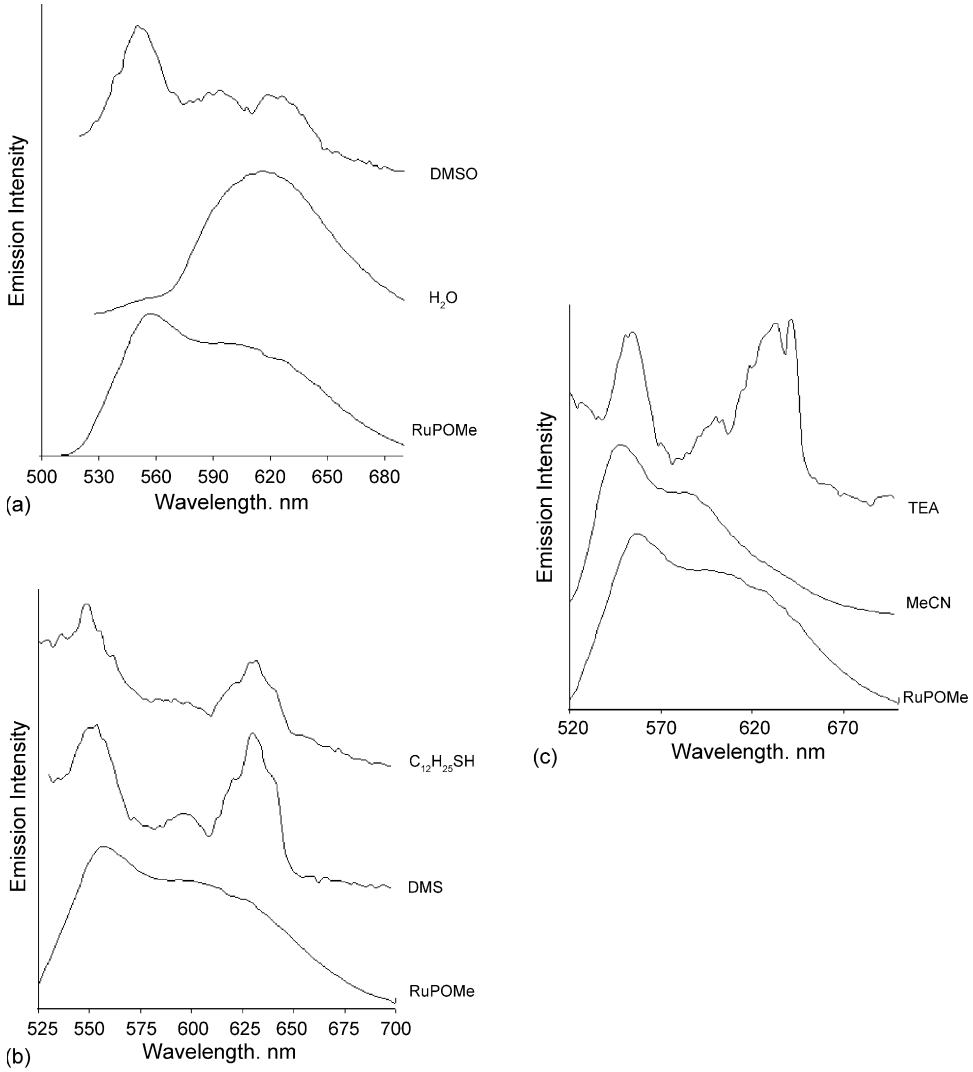

Fig. 9. Emission of (**1**) with 100 equivalents of various small molecules. (a) O-bound, (b) S-bound, (c) N-bound, measurements were taken in a 4:1 EtOH:MeOH solution at ~77 K.

Table 2
Lever parameters (E_L) [83] for selected ligands listed as potentials in volts vs. NHE = −0.240 V vs. SCE

Ligand	E_L (V)
Cl^-	−0.24
H_2O	0.04
Ph_3P	0.39
Me_2O	0.45
POMe	0.63[a]
bpy	0.259

[a] Calculated from $E_{1/2}(Ru^{III/II})_{calc} = 0.97[\sum E_L] + 0.04$ [77] using $RuCl_2$(POMe-P,O)$_2$, $E_{1/2}(Ru^{III/II}) = 0.80$ V vs. NHE [73].

3.2.3. Ligand influenced energy gap

A helpful parameter for evaluating ligand effects on coordination complex energetics was introduced by Gutmann [71]. The solvent donor number (DN) is calculated calorimetrically to be the negative of the heat of formation for the donor solvent (D) with $SbCl_5$ in an inert solvent (highly dilute so as to approximate gas phase conditions) [70]. This quantifies the observation by Briegleb that the donor strength of a molecule is represented by its ionization energy [72]. Gutmann explained the donor number as an expression of the total amount of interaction with an acceptor molecule, including contributions by dipole–dipole or dipole–ion interactions and by the binding effect caused by the availability of the free electron pair [71]. Gutmann solvent donor numbers for the ligands under consideration in this section are reported in Table 1.

The Gutmann solvent donor numbers correlate well to the observed absorbance shifts that are observed for (**1**) with various small molecule donors. When the MLCT absorbance maximum is plotted against the donor number, a linear plot emerges (Fig. 8). As the solvent donor number increases, the electron density at the metal center increases, destabilizing the HOMO and causing a red shift in the MLCT band. This explains the red shift of (**1**·**L**) that is observed with the increasing solvent donor number of **L**.

3.2.4. Emission properties of (1·L)

Low temperature emission studies with (**1**) in 2:1 ethanol/acetone at relatively high concentrations displayed ligand dependent energetic shifts. The result is a beautiful array of emission colors in the presence of varying small molecules ranging from cherry brown in the presence of triethylamine to yellow in the presence of acetonitrile to olive in the presence of dodecanethiol [73]. Emission spectra have been obtained for (**1**·**L**) with five of the ligand donor molecules evaluated in the absorbance discussion. In each case the emission spectra for the bound ligand complexes (**1**·**L**), appeared to be in equilibrium with the parent compound (**1**) (Fig. 9). By analogy with the previously studied (**1**·H_2O) system, the lower energy band was assigned to the ligand-bound complex.

The emission maxima for these bound ligand complexes (**1**·**L**), do not show a linear correlation with the Gutmann solvent donor numbers. Although a specific trend cannot be established between the ligand properties and emission energies of (**1**·**L**), it has been observed that when the labile ether functional group of (**1**) is displaced by a small molecule, the energy of the MLCT emission band is red shifted. When a small molecule coordinates to the metal center, the bidentate P,O-chelate is opened and we propose that the metal–ligand orbital overlap of the ruthenium–phosphine dπ* orbital will change [62]. This change in overlap would affect the electron density at the ruthenium center, decreasing the π backbonding interaction and causing a change in the ruthenium HOMO depending on the Lever parameter of the incoming ligand/solvent. The observed result is a decrease in the energy of the MLCT emission band. The bound ligand complexes (**1**·**L**) emission bands appear at longer wavelengths than the emission of the parent P,O-complex (**1**).

3.2.5. Electrochemical behavior and optical energy correlation

Ground state reduction potentials can be used to calculate information regarding the luminescent excited state as demonstrated by Lever [74,75]. Lever parameters (E_L) can be used to calculate an approximate contribution of the ligands to the redox potential, $\Delta E_{(redox)}$, of a complex. The energy of the MLCT absorption, which corresponds to $Ru^{II}(bpy) \rightarrow Ru^{III}(bpy^{\bullet -})$, scales linearly with the difference between the $Ru^{III/II}$ and $bpy^{0/-}$ redox couples, $\Delta E_{(redox)}$ [76,77]. Adjusted for the Stokes shift, the same holds true for the emission energies. These relationships have been used as confirmation that, within families

Table 3
Reduction potentials for (**1**) and sensor–analyte complex (**1**·H_2O)

Complex	Observed (V vs. SCE)			Predicted				
	E_{ox}	E_{red}	$\Delta E_{(redox)}$	$E_{1/2}(Ru^{III/II})_{calc}$[a]	$E_{1/2}(bpy^{0/-})_{calc}$[b]	$\Delta E_{(redox)calc}$[c]	$E_{abs}(MLCT)_{calc}$[d]	$E_{em}(0-0)_{calc}$[e]
1	1.56[f]	−1.27[f]	2.83	1.42	−1.35	2.77	2.98	2.25
1·OH_2	–	–	–	1.23	−1.40	2.63	2.84	2.14
$Ru(bpy)_3^{2+}$	1.23[g]	−1.35[g]	2.58			2.61[h]	2.74[h]	2.12[h]

[a] $E_{1/2}(Ru^{III/II})_{calc} = 0.97[\sum E_L] + 0.04$ [77].
[b] $E_{1/2}(bpy^{0/-})_{calc} = 0.25(\pm 0.01)[\sum E_L(bpy)] - 1.40(\pm 0.03)$ [73].
[c] $\Delta E_{(redox)calc} = E_{1/2}(Ru^{III/II})_{calc} - E_{1/2}(bpy^{0/-})_{calc}$.
[d] $E_{abs}(MLCT) = 1.00\ \Delta E_{(redox)} + 0.21$ [76].
[e] $E_{em}(0-0) = 0.76(\pm 0.06)\Delta E_{(redox)} + 0.14(\pm 0.04)$ [84].
[f] CH_2Cl_2, 0.1 M [*n*-Bu_4N]PF_6, 25 °C.
[g] CH_3CN, 0.1 M [*n*-Et_4N]PF_6, 25 °C [85].
[h] These values were calculated from emission and absorbance data.

Table 4
Observed vs. predicted MLCT absorption energy and highest energy emission (eV) for (**1**) and sensor–analyte complexes, **1**·**L** in a 3.0×10^{-5} M solution of (**1**) with 100 equivalents of (**L**)

Complex	E_{abs}(MLCT)		E_{em}(0–0)		
	Observed	Predicted[a]	Observed[b]	Predicted[c]	Predicted[d]
1	2.97	2.98	2.23	3.48	2.42
1·MeCN	3.01	3.06	2.13	3.58	2.50
1·NEt_3	2.69	2.88	1.96	3.35	2.37
1·DMSO-S	–	3.15	2.09[e]	3.70	2.50
1·DMSO-O	2.97[e]	2.79	1.99[e]	3.23	2.32
1·Me_2S	2.98	3.03[f]	1.97	3.55[f]	2.44[f]
1·OH_2	2.88[g]	2.84	2.02[g]	3.29	2.35

(Solvent: 4:1 EtOH:MeOH) [73].
[a] Calculated from $\Delta E_{(redox)calc}$ using $E_{abs}(MLCT) = 1.00\Delta E_{(redox)} + 0.21$.
[b] May not be true 0–0 band.
[c] Calculated from $\Delta E_{(redox)calc}$ using $E_{em}(0–0) = 0.76(\pm0.06)\Delta E_{(redox)} + 0.14(\pm0.04)$, trend for all Ru(II) bpy complexes.
[d] Calculated from $\Delta E_{(redox)calc}$ using $E_{em}(0–0) = 0.49(\pm0.03)\Delta E_{(redox)} + 1.06(\pm0.01)$, trend for $[Ru(bpy)(biq)LL']^{2+}$ complexes.
[e] Measured from samples containing both **1**·DMSO-*S* and **1**·DMSO-*O*.
[f] Approximated as Me_2S.
[g] More than 100 equivalents of H_2O present.

of Ru(II) bpy complexes, the absorption and emission arise from analogous MLCT and LMCT processes. Excellent discussions of these relationships are available in reviews by Lever [78–80].

Lever parameters (Table 2) have been used to estimate the redox potentials, $\Delta E_{(redox)}$, for (**1**) and (**1**·**L**). The solution electrochemistry of the sensor complex was examined via cyclic voltammetry for (**1**) to compare to the predicted value. The experimentally observed and predicted values of $\Delta E_{(redox)}$ are listed in Table 3.

The predicted absorbance and emission energies for a series of complexes (**1**·**L**), based on Lever parameters have been calculated and compared to the observed optical energies obtained from previous sections in Table 4 [73]. The Lever predicted values for absorbance are well matched to the values obtained experimentally (the average difference between the calculated and observed values is 0.09 eV). However, the emission differences are much larger, even when two different equations are employed following trends for both Ru(II) bpy complexes and $[Ru(bpy)(biq)LL']^2$ complexes. It is likely that this difference in energy is the result of distortions in the excited state and difficulty in assigning the true $E_{0–0}$ value for the relatively broad MLCT bands in the optical spectra.

3.2.6. Lifetime studies

Excited state lifetimes were determined for complexes (**1**), (**2**), (**2**·H_2O) and (**1**·**L**) by time-resolved emission measurements following laser excitation at 337 nm. As the temperature increases, a decrease in the lifetime of luminescence is observed for both (**1**) and (**2**). This result is consistent with thermal population of the non-radiative d–d states as described previously for MLCT complexes of Ru(II) [62]. The lifetime of the MLCT emission becomes shorter as the rate of energy transfer to the d–d state increases.

Table 5
77 K lifetime values for several complexes (1·**L**), monitored at the wavelength of maximum signal intensity

Complex	τ (77 K)[a]
(**1**)	4.19 ± 0.05 μs at 620 nm
(**1**·MeCN)	7.89 ± 0.05 μs at 552 nm
(**1**·TEA)	7.18 ± -0.05 μs at 550 nm
(**1**·DMS)	2.80 ± 0.05 μs at 625 nm
(**1**·DMSO)	6.66 ± 0.05 μs at 550 nm
(**2**)	3.24 ± 0.05 μs at 620 nm
(**2**·H_2O)	0.22 ± 0.05 μs at 620 nm

Values were determined assuming a first order rate decay process.
[a] Monitored at wavelength of maximum signal intensity.

The lifetimes of (**1**), (**2**), (**2**·H_2O) and (**1**·**L**) were measured at the wavelength of maximum signal intensity (Table 5). While a distinct trend appears to be missing in these results, we note that the lifetime of (**2**·H_2O) is less than the lifetime of (**2**). However, except for (**1**·DMS), all of the lifetime values recorded for (**1**·**L**) were longer than that of (**1**). It appears that the two samples that were monitored at 620 and 625 nm had significantly shorter lifetimes than the samples that were monitored around 550 nm. This difference may be explained by the fact that the ~620 nm band reports the lifetime of the complex (**1**·**L**), and the ~550 nm band reports the lifetime of (**1**) itself. Thus it could be generally stated that the 77 K lifetime of the ligand substituted hemilabile complexes (**1**·**L**) and (**2**·**L**) are shorter than the corresponding ether bound complexes.

When a small molecule binds to the ruthenium center of the hemilabile complexes, the phosphine–ether ligand becomes a monodentate phosphine. The increased molecular flexibility appears to result in an increase in the manifold of medium to low frequency d–d states capable of coupling to the solvent (Fig. 10). The rate of vibrational relaxation from the d–d state is therefore more rapid in the aquo-complexes. The more accessible non-radiative d–d state shortens the observed lifetime of luminescence from the MLCT state.

3.2.7. Temperature-dependent lifetime studies as kinetics probe

Temperature-dependent lifetimes for (**1**), (**2**) and (**1**·**L**) were fit to the expression below using a non-linear least-squares procedure [62].

$$\frac{1}{\tau(T)} = k + k'^{0} \exp\left(\frac{-\Delta E'}{RT}\right) \quad (1)$$

In Eq. (1) $k = k_r + k_{nr}$; k_r and k_{nr} are the rate constants for the nominally temperature-independent radiative and non-radiative decay processes, respectively; k'^0 is the thermally activated process prefactor with activation energy $\Delta E'$; k' is equal to this temperature dependent term, $k'^0 \exp(-\Delta E'/RT)$, and R is the ideal gas constant.

Experimental determination of the fluorescence lifetimes at different temperatures allows for the determination of the thermal activation energy barrier and the rate of energy transfer from the ^{3}MLCT → d–d state. As expected, the ^{3}MLCT → d–d activation energy barrier, $\Delta E'$, is greater for $[Ru(bpy)_3](PF_6)_2$ than

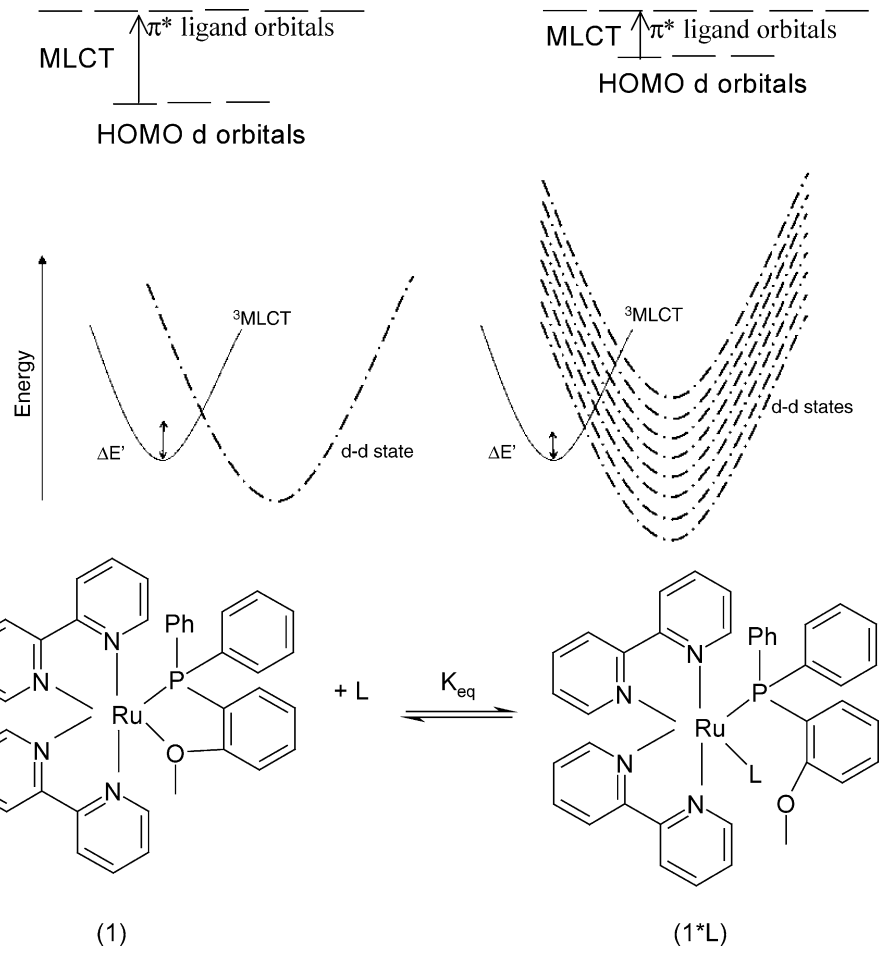

Fig. 10. Differences in the ligand field splitting parameter of (**1**) and (**1**·**L**) due to changed overlap of the Ru–phosphine dπ^* overlap, resulting in less π backbonding.

Table 6
Excited state decay parameters for (**1**) and (**2**)

Complex	Concentration (M)	k (s^{-1})	k'^0 (s^{-1})	$\Delta E'$ (cm^{-1})	k' (s^{-1}, 298 K)	k' (s^{-1}, 77 K)
$[Ru(bpy)_3](PF_6)_2$ in CH_2Cl_2 [85]	–	4.1×10^5	4.5×10^{13}	3560	1.54×10^6	5.802×10^{-16}
RuPOMe (**1**) in 4:1 ethanol: methanol	3.0×10^{-5}	2.5×10^5	3.0×10^{11}	1390	3.65×10^8	1.568
RuPOEt (**2**) in 4:1 ethanol: methanol	3.0×10^{-5}	2.5×10^5	3.0×10^{10}	1147	1.18×10^8	14.761

The values were obtained by fitting the lifetime to the expression in Eq. (1).

(**1**) or (**2**) (Table 6). The efficient pathway of non-radiative decay through the d–d state and the smaller activation energy barrier for (**1**) and (**2**), results in no emission at ambient temperatures. This also explains the several-fold increase in the non-radiative decay rate, k', of (**1**) and (**2**) relative to $[Ru(bpy)_3](PF_6)_2$.

Temperature dependent lifetime studies were also conducted for several complexes (**1**·**L**). The resulting $-\ln(\tau)$ versus $1/T$ plots with the fitted Eq. (1) are shown for (**1**·MeCN), (**1**·TEA), (**1**·DMS) and (**1**·DMSO) in Fig. 11. From these values, the rates of energy transfer from the MLCT to d–d state, k', and the thermal activation energy barrier, ΔE, were calculated, Table 7.

In all instances of (**1**·**L**), ΔE is significantly smaller and k' distinctly faster than for (**1**). These results are in agreement with our understanding that as the hemilabile ligand undergoes the transition from bidentate to monodentate, the increased molecular flexibility results in an increased manifold of d–d states that are available to vibronically couple to the solvent. This increased manifold of d–d states results in a lowering of the activation energy barrier for non-radiative decay from the ^{3}MLCT to d–d state. An increase in the rate of non-radiative decay is also a

Table 7
Energy transfer rates and thermal activation energy barrier data for (**1**) with small molecules

Ligand	k'^0 (s^{-1})	k' (s^{-1}, 77 K)	ΔE (cm^{-1})
(**1**)	3.0×10^{11}	1.735	1390.28
(**1**·MeCN)	2.00×10^9	1235.52	782.05
(**1**·TEA)	2.00×10^9	476.78	834.14
(**1**·DMS)	2.00×10^9	765.95	813.34
(**1**·DMSO)	1.85×10^9	1274.18	768.21

Values were calculated using Eq. (1).
$k' = k'^0 \exp(-\Delta E'/RT)$. All experiments were run in 4:1 ethanol:methanol.

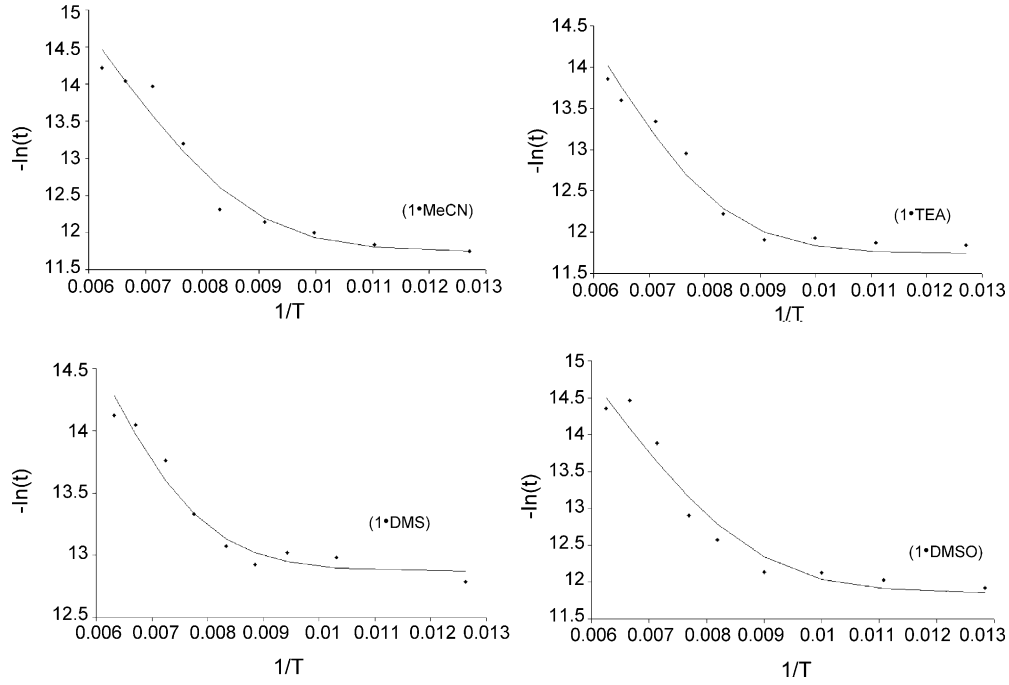

Fig. 11. Temperature-dependent lifetime plots for various complexes (**1**·**L**) The resulting data was fit (fit line shown) to Eq. (1) yielding numerical values for k, k'^{0} and $\Delta E/R$. Hundred equivalents of **L** were present in 3.0×10^{-5} M (**1**) in 4:1 EtOH:MeOH solution. The sum square of the residuals for the fit of Eq. (1) to the data are as follows: (**1**·MeCN), 0.087; (**1**·TEA), 0.198; (**1**·DMS), 0.093; (**1**·DMSO), 0.40.

direct result of the increased manifold of d–d states in the (**1**·**L**) complexes as the thermal activation energy barrier is lowered and more pathways are available for vibrational relaxation from the d–d state.

4. Conclusion

We have demonstrated that hemilabile ligand complexes are promising chemosensors based on their reversible ligand-dependent fluorescence response. Our understanding of the ligand effects on coordination complex energy levels has been advanced in significant ways. It has been shown that the MLCT energy of the Ru(II) coordination complex containing two bipyridine ligands and one phosphine ether ligand is greater than the corresponding Ru(II) complex with three bipyridine ligands. This increase in the emission energy is attributed to stabilization of the metal d-based HOMO orbitals caused by the backbonding effect observed in the presence of the π-accepting phosphine ligand.

It has also been suggested that when the phosphine ether ligand detaches at the labile position, the metal–ligand orbital overlap of the ruthenium–phosphine $d\pi^*$ state is affected. This results in a decreased π backbonding interaction and destabilization of the d-orbital based HOMO orbitals. This is consistent with the generally observed decrease in the metal-to-ligand energy gap of (**1**·**L**) and was especially pronounced in the case of (**1**·H_2O) and (**1**·TEA). The ligand influence on the metal-to-ligand energy gap was observed to follow a trend in the Gutmann donor numbers. This trend indicates that ligands that are strong electron donors raise the metal-based HOMO. This trend was also consistent with the incoming ligand having a Lever parameter, E_L that was substantially larger than the ether, which is being displaced.

A switch of the phosphine–ether ligand from bidentate to monodentate upon binding of a small molecule ligand (**L**) results in a decrease in the activation energy barrier, $\Delta E'$, and an increase in the rate, k'. These photophysical changes are attributed to an increased manifold of d–d states that are capable of coupling to the solvent. The increased manifold of d–d states result from the increase in molecular flexibility that occurs when the labile portion of the hemilabile ligand detaches from the metal center.

In conclusion, the hemilabile complexes (**1**) and (**2**), show promise as chemosensors based on the reported photochemical changes caused by the binding of small molecule analytes. These results successfully demonstrate that the rate of non-radiative decay from the ligand-field d–d state in hemilabile ligand complexes can be modified through substitution at the labile portion of the bidentate ligand. We describe this as "tunable ligand field deactivation."

Acknowledgements

We thank Szu-Wei Yang of Binghamton University for instrumental support and, Dr. Brendan Flynn, Dr. Cliff Timpson and Dr. Stanley K. Madan for useful discussions. The authors would also like to thank the reviewers for very useful suggestions. S.E.A., Y.Z. and W.E.J. acknowledge the NSF GK-12 program and NIH (1R15ES10106) for funding. M.O.W. and C.W.R. acknowledge NSERC of Canada for funding.

References

[1] D.T. McQuade, A.E. Pullen, T.M. Swager, Chem. Rev. 100 (2000) 2537.
[2] R. Martinez-Manez, F. Sancenon, Chem. Rev. 103 (2003) 4419.
[3] K. Severin, Coord. Chem. Rev. 245 (2003) 3.
[4] X. Cui, H.M. Carapuca, R. Delgado, M.G.B. Drew, V. Felix, J. Chem. Soc., Dalton Trans. 11 (2004) 1743.
[5] T.W. Lewis, G.G. Wallace, M.R. Smyth, Analyst 124 (3) (1999) 213.
[6] H.Z. Bu, S.R. Mikkelson, A.M. English, Anal. Chem. I67 (1995) 4071.
[7] E.J. Calvo, C. Danilowicz, L. Diaz, J. Chem. Soc., Faraday Trans. 89 (1993) 377.
[8] T. Kaku, H.I. Kiran, Y. Okamoto, Anal. Chem. 67 (1995) 4071.
[9] F. Bedioui, J. Devynck, C. Bied-Charreton, Acc. Chem. Res. 28 (1995) 30.
[10] B.R. Saunders, R.J. Fleming, K.S. Murray, Chem. Mater. 7 (1995) 1082.
[11] M.H. Lee, Y.T. Hang, S.B. Rhee, Synth. Met. 69 (1995) 515.
[12] L. Wang, E. Kobatake, Y. Ikiriyama, M. Aizawa, Denki Kagaku 60 (1992) 1050.
[13] J. Chen, A.K. Burrell, G.E. Collis, D.L. Officer, G.F. Swiegers, C.O. Too, G. Wallace, Electrochim. Acta 47 (17) (2002) 2715.
[14] L. Chen, D.W. McBranch, H. Wang, R. Helgeson, F. Wudl, D.G. Whitten, PNAS 96 (22) (1999) 12287.
[15] G. Absalan, M. Soleimani, M. Asadi, M.B. Ahmadi, Anal. Sci. 20 (10) (2004) 1433.
[16] D.J. David, M.C. Willson, D.S. Ruffin, Anal. Lett. 9 (1976) 389.
[17] A.L.L. Duchateau, M.G. Hillemans-Crombach, A. Astrid van Duijnhoven, R. Reiss, T. Sonke, Anal. Biochem. 330 (2004) 362.
[18] E.A. Garcia, R.G. Fernandez, M.E. Diaz-Garcia, Microporous Mesoporous Mater. 77 (2–3) (2005) 235.
[19] K. Takato, N. Gokan, M. Kaneko, J. Photochem. Photobiol., A: Chem. 169 (1) (2004) 109.
[20] M.E. Padilla-Tosta, J.M. Lloris, R. Martines-Manes, M. Marcos, M. Dolores, A. Miguel, T. Pardo, F. Sancenon, Soto, Eur. J. Inorg. Chem. 6 (2001) 1475.
[21] R. Grigg, W.D.J.A. Norbert, Chem. Commun. (1992) 1300.
[22] B. Valeur, I. Leray, Coord. Chem. Rev. 20 (2000) 3.
[23] G. Klein, D. Kaufmann, S. Schurch, Reymond, J. Chem. Commun. (2001) 561.
[24] A. Ohshima, A. Momotakeb, T. Araia, Tetrahedron Lett. 45 (2004) 9377.
[25] M. Narita, Y. Higuchi, F. Hamada, H. Kumagai, Tetrahedron Lett. 39 (1998) 8687.
[26] L. Fan, Y. Zhang, W.E. Jones Jr., Macromolecules 38 (2005) 2844.
[27] A.P. de Silva, H.Q.N. Gunaratne, T. Gunnlaugsson, A.J.M. Huxley, C.P. McCoy, J.T. Rademacher, T.E. Rice, Chem. Rev. 97 (5) (1997) 1515.
[28] R. Martinez-Manez, F. Sancenon, Chem. Rev. 103 (2003) 4419.
[29] Y. Zhang, C. Murphy, W.E. Jones Jr., Macromolecules 35 (2002) 630.
[30] C.B. Murphy, Y. Zhang, T. Troxler, V. Ferry, J.J. Martin, W.E. Jones, J. Phys. Chem. B 108 (2004) 1537.
[31] J. Kim, D.T. McQuade, S.K. McHugh, T.M. Swager, Angew. Chem. Int. Ed. 39 (21) (2000) 3868.
[32] B. Wang, M.R. Wasielewski, J. Am. Chem. Soc. 119 (1997) 12.
[33] L.X. Chen, W.J.H. Jager, D.J. Gostola, M.P. Niemczyk, M.R. Wasielewski, J. Phys. Chem. B 104 (2000) 1950.
[34] L.X. Chen, W.J.H. Jager, D.J. Gostola, M.P. Niemczyk, M.R. Wasielewski, Synth. Met. 116 (2001) 229.
[35] C. Tan, E. Atlas, J.G. Muller, M.R. Pinto, V.D. Kleiman, K.S. Schanze, J. Am. Chem. Soc. 126 (42) (2004) 13686.
[36] D.A. Weinberger, T.B. Higgins, C.A. Mirkin, L.M. Liable-Sands, A.L. Rheingold, Angew. Chem. Int. Ed. 38 (17) (1999) 2565.
[37] D.A. Weinberger, T.B. Higgins, C.A. Mirkin, C.L. Stern, L.M. Liable-Sands, A.L. Rheingold, J. Am. Chem. Soc. 123 (2001) 2503.
[38] J.C. Jeffrey, T.B. Rauchfuss, Inorg. Chem. 18 (10) (1979) 2658.
[39] C.S. Slone, D.A. Weinberger, C.A. Mirkin, The transition metal coordination of hemilabile ligands, in: K.D. Karlin (Ed.), Progress in Inorganic Chemistry, vol. 48, John Wiley & Sons Inc., New York, 1999, p. 233.
[40] C.W. Rogers, Y. Zhang, B.O. Patrick, W.E. Jones Jr., M.O. Wolf, Inorg. Chem. 41 (2002) 1162.
[41] J.I. Dulebohn, S.C. Haefner, K.A. Berglund, K.R. Dunbar, Chem. Mater. 4 (1992) 506.
[42] A. Bader, E. Lindner, Coord. Chem. Rev. 108 (1991) 27.
[43] E. Lindner, S. Pautz, M. Haustein, Coord. Chem. Rev. 155 (1996) 145.
[44] P. Baunstein, F. Naud, Angew. Chem. Int. Ed. 40 (2001) 680.
[45] P. Das, M. Sharma, N. Kumari, D. Dutta, D. Kumar, Indian J. Chem. 41 (2002) 560.
[46] S. Jung, C.D. Brandt, H. Werner, New J. Chem. 25 (2001) 1101.
[47] E. Lindner, J. Wald, K. Eichele, R. Fawzi, J. Organomet. Chem. 601 (2000) 220.
[48] J.I. Dulebohn, S.C. Haefner, K.A. Berglund, K.R. Dunbar, Chem. Mater. 4 (1992) 506.
[49] C.W. Rogers, M.O. Wolf, Chem. Commun. (1999) 2297.
[50] K. Kalyanasundaram, M. Gratzel, Coord. Chem. Rev. 177 (1998) 347.
[51] A.P. de Silva, D.B. Fox, A.J.M. Huxley, N.D. McClenaghan, Roiron, J. Coord. Chem. Rev. 186 (1999) 297.
[52] B. Jiang, S.W. Yang, S.L. Bailey, L.G. Hermans, R.A. Niver, M.A. Bolcar, W.E. Jones Jr., Coord. Chem. Rev. 171 (1998) 365.
[53] C.W. Rogers, B.O. Patrick, S.J. Rettig, M.O. Wolf, J. Chem. Soc., Dalton Trans. (2001) 1278–1283.
[54] G.A. Crosby, W.G. Perkins, D.M. Klassen, J. Chem. Phys. 43 (1965) 1498.
[55] R.W. Harrigan, G.A. Crosby, J. Chem. Phys. 59 (1973) 3468.
[56] F. Felix, J. Ferguson, H.C. Gudel, A. Ludi, J. Am. Chem. Soc. 102 (1980) 4096.
[57] F. Boletta, A. Juris, M. Maestri, D. Sandrini, Inorg. Chem. Acta 44 (1980) L175.
[58] J.N. Demas, D.G. Taylor, Inorg. Chem. 18 (1979) 3177.
[59] J. Van Houten, R.J. Watts, J. Am. Chem. Soc. 98 (1976) 4853.
[60] F. Barigelletti, P. Belser, A. von Zelewsky, A. Juris, V. Balzani, J. Phys. Chem. 89 (1985) 3680.
[61] G.A. Crosby, Acc. Chem. Res. 8 (1975) 231.
[62] J.V. Caspar, T. Meyer, J. Inorg. Chem. 22 (1983) 2444.
[63] T.J.J. Kinnunen, M. Haukka, E. Pesonen, T. Pakkanen, J. Organomet. Chem. 655 (2002) 31.
[64] V. Balzani, A. Juris, F. Barigelletti, P. Belser, A. Von Zelewsky, Scientific Papers of the Institute of Physical and Chemical Research (Japan), vol. 78, 1984, p. 78.
[65] R.S. Lumpkin, E.M. Kober, L.A. Worl, Z. Murtaza, T.J. Meyer, J. Phys. Chem. 94 (1990) 239.
[66] P.A. Anderson, F.R. Keene, T.J. Meyer, J.A. Moss, G.F. Strouse, J.A. Treadway, J. Chem. Soc., Dalton Trans. (2002) 3820.
[67] G.H. Allen, R.P. White, D.P. Rillema, T.J. Meyer, J. Am. Chem. Soc. 106 (1984) 2613.
[68] S.E. Angell, Y. Zhang, C.W. Rogers, M.O. Wolf, W.E. Jones Jr., Inorg. Chem. 44 (21) (2005) 7377.
[69] R.J. Crutchley, A.B.P. Lever, Inorg. Chem. 21 (1982) 2276.
[70] D.M. Roundhill, Photochemistry and Photophysics of Metal Complexes, Plenum Press, New York, 1994.
[71] V. Gutmann, Coordination Chemistry in Non-Aqueous Solutions, Springer-Verlag, New York, 1968.
[72] G. Briegleb, Elektronen-Donator-Akzeptor-Komplexe, Springer-Verlag, Berlin, Gottingen, Heidelberg, 1961.
[73] C. Rogers, A Hemilabile Ligand Approach to Ruthenium-based Luminescent Molecular Sensors, University of British Columbia, Vancouver, British Columbia, 2001.
[74] K. Kalyanasundaram, Coord. Chem. Rev. 46 (1982) 159.
[75] K. Kalyanasundaram, Photochemistry of Polypyridine and Porphyrin Complexes, Academic Press, London, 1992.
[76] E.S. Dodsworth, A.B.P. Lever, Chem. Phys. Lett. 124 (1986) 152.
[77] A.B.P. Lever, Inorg. Chem. 29 (1990) 1271.
[78] A.B.P. Lever, E.S. Dodsworth, Electrochemistry, charge transfer spectroscopy, and electronic structure, in: E.I. Solomon, A.B.P. Lever (Eds.), Inorganic Electronic Structure And Spectroscopy, vol. II, John Wiley & Sons Inc., New York, 1999, pp. 227–289, Applications and Case Studies.

[79] E.S. Dodsworth, A.A. Vlcek, A.B.P. Lever, Inorg. Chem. 33 (1994) 1045.
[80] A.B.P. Lever, Can. J. Anal. Sci. Spec. 42 (1997) 22.
[81] Y.J. Chen, C.H. Kao, S.J. Lin, C.C. Tai, K.S. Kwan, Inorg. Chem. 39 (2000) 189.
[82] Pure Appl. Chem. 75(1) (2003). 71.
[83] L. Perrin, E. Clot, O. Eisenstein, J. Loch, R.H. Crabree, Inorg. Chem. 40 (2001) 5806.
[84] A.A. Vlcek, E.S. Dodsworth, W.J. Pietro, A.B.P. Lever, Inorg. Chem. 34 (1995) 1906.
[85] J.V. Caspar, T.J. Meyer, J. Am. Chem. Soc. 105 (1983) 5583.